Magneto-transport studies on $(Pr_{1/3}Sm_{2/3})_{2/3}A_{1/3}MnO_3$ (A = Ca, Sr and Ba) compounds

Magneto-transport studies on $(Pr_{1/3}Sm_{2/3})_{2/3}A_{1/3}MnO_3$ (A = Ca, Sr and Ba) compounds

Saket Asthana[1], D Bahadur[1], A K Nigam[2] and S K Malik[2]

[1] Department of Metallurgical Engineering and Materials Science, Indian Institute of Technology, IIT Bombay, Powai, Mumbai 400076, India
[2] Tata Institute of Fundamental Research, Colaba, Mumbai 400005, India

Abstract
The magnetic and transport properties of $(Pr_{1/3}Sm_{2/3})_{2/3}A_{1/3}MnO_3$ (A = Ca, Sr and Ba) compounds, prepared by the citrate-gel route, have been investigated. These compounds are found to crystallize in the orthorhombic structure. Charge ordering transport behaviour is indicated only in the Ca-substituted compound. The Sr- and Ba-substituted compounds show a metal–insulator transition and semiconducting-like behaviour, respectively. The magnetoresistance is highest in the Ba-substituted compound. All three samples show irreversibility in magnetization as a function of temperature in zero-field cooled (ZFC) and field cooled (FC) plots. Non-saturating magnetization, even at 5 K and 4 T field, is observed in Ca- as well Ba-substituted compounds.

1. Introduction

The mixed valency perovskite manganites of the general formula $Ln_{1-x}A_xMnO_3$ (Ln = rare earth and A = divalent alkaline earth cation) have created a great deal of interest because of their colossal magnetoresistance (CMR) behaviour. These systems also have technological importance such as in sensor applications, and especially for increasing data storage by increasing the sensitivity of hard disk drive read heads [1, 2]. These manganites become ferromagnetic (FM) at an optimal value of x (or Mn^{4+} content) and undergo a metal–insulator (MI) transition around the ferromagnetic transition temperature. The effects of divalent alkaline-earth element substitution in the stoichiometric perovskite manganites $Ln_{1-x}A_xMn_{1-y}M_yO_3$ have been extensively studied [3–5]. These studies show that the Curie temperature, T_C, and the magnetoresistance are optimized for Mn^{4+} content of about 33%. These properties are attributed to the double exchange (DE) interaction associated with electron hopping from Mn^{3+} to Mn^{4+}. The double exchange interaction, which favours itinerant electron behaviour, is opposed by the Jahn–Teller (JT) distortion of the Mn^{3+}. Recent studies

have shown that DE alone cannot explain the observed behaviour in manganites [6] and other effects also play an important role. These include charge ordering, average A-site cationic radius $\langle r_A \rangle$ [7, 8], A-size cationic size mismatch [9, 10], oxygen deficiency [11], electron–lattice coupling [12], polaron effect due to strong electron–phonon interaction arising from the Jahn–Teller distortion [6], etc. The average size of the A-site cation of these perovskites and the size mismatch at the A-site modify the Mn–O–Mn bond angle and affect the e_g electron hopping between Mn^{3+} and Mn^{4+} degenerate states. The effect of ionic size variation can also be understood by the tolerance factor defined as $t = (\langle r_A \rangle + r_O)/\sqrt{2}(r_B + r_O)$, where r_O and r_B are the radii of the oxygen and the B-site transition metal ions, respectively.

The electronic properties of the manganites can be tuned either by substituting cations at the A- or B-sites or by varying the oxygen content in the regular perovskite structure [13–15]. The A-site cation is responsible for the structural distortions while the B-site cation is responsible for the magnetic interactions. Mixing cations of different charges at the A-site is the most straightforward experimental method for systematically tuning the properties of these materials. There are many ways to achieve this with Ln^{3+}/M^{2+} combinations (Ln = rare earth and M = Ca, Ba Sr and Pb) or with rare earth ion combinations. This has led to efforts to unify the properties of compositions from different chemical phase diagrams within a single framework by using a simple ionic description of the A-site cations [16].

A lot of work has been done on manganites with a single rare earth ion at the A-site. In the present work, we have undertaken to substitute two rare earth ions, namely Pr and Sm, at the A-site in a fixed ratio, and to vary the alkaline earth ion. In this context, we have chosen the series $(Pr_{1/3}Sm_{2/3})_{2/3}A_{1/3}MnO_3$ (A = Ca, Sr and Ba) for our present studies.

2. Experimental details

Polycrystalline $(Pr_{1/3}Sm_{2/3})_{2/3}A_{1/3}MnO_3$ (A = Ca, Sr and Ba) samples were synthesized by the chemical citrate-gel route using high purity Pr_6O_{11}, Sm_2O_3, $CaCO_3$, $BaCO_3$, $SrCO_3$ and manganese acetate. The as-prepared powders were calcined at 1000 °C in air for 2 h. The powders were pelletized in the form of rectangular bars and sintered at 1200 °C in air. X-ray diffraction patterns of the samples were recorded using Cu Kα radiation (PW 3040/60 Philips, PANalytical). Resistivity measurements at different applied magnetic fields were carried out from 320 to 5 K using the standard four-probe dc method (PPMS, Quantum Design). Magnetic measurements were made using a vibrating sample magnetometer (Oxford, Maglab VSM) at different fields and in the temperature range 300–5 K.

3. Results and discussion

3.1. Crystal structure

Figure 1 shows the x-ray diffraction patterns for $(Pr_{1/3}Sm_{2/3})_{2/3}A_{1/3}MnO_3$ (A = Ca, Sr and Ba) compositions. All the lines in the patterns could be indexed on the basis of an orthorhombic structure (space group *Pnma* No. 62). In the Ca-substituted sample, splitting of some of the x-ray lines is observed which is due to increased orthorhombicity of this compound (compared to that of the other two). This in turn is due to smaller ionic size of the Ca ion (1.18 Å) in comparison to those of Sr (1.31 Å) and Ba (1.47 Å) ions. The average A-site ionic radius, $\langle r_A \rangle$ varies from 1.158 Å for Ca-, 1.202 Å for Sr- and 1.255 Å for Ba-substituted samples. The mean radius has been calculated using the coordination number nine [17]. The tolerance factors for Ca-, Sr-, and Ba-containing compounds are 0.9018, 0.9173 and 0.9360, respectively.
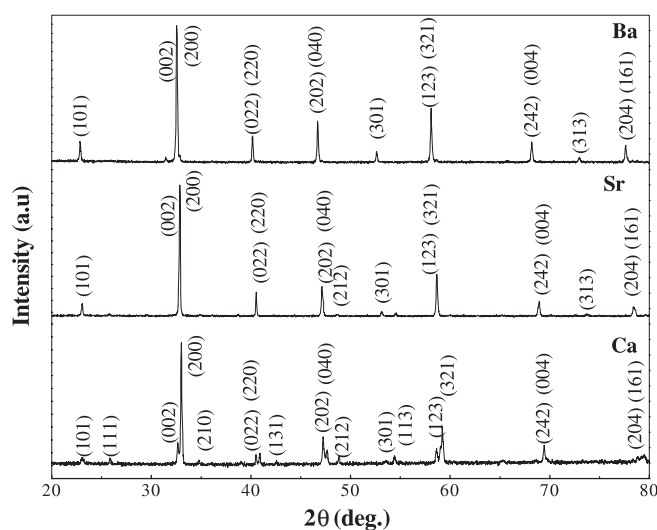
Figure 1. X-ray diffraction patterns of the series $(Pr_{1/3}Sm_{2/3})_{2/3}A_{1/3}MnO_3$ (A = Ca, Sr and Ba) showing the single phase nature of the compounds.

Table 1. Refined lattice parameters using the Rietveld method, tolerance factors, and T_C for the series $(Pr_{1/3}Sm_{2/3})_{2/3}A_{1/3}MnO_3$ (A = Ca, Sr and Ba).

| Systems	a (Å)	b (Å)	c (Å)	V (Å^3)	t	T_C (K)
$(Pr_{1/3}Sm_{2/3})_{2/3}Ca_{1/3}MnO_3$	5.4780(7)	7.6501(0)	5.4067(8)	226.58(5)	0.9018	40
$(Pr_{1/3}Sm_{2/3})_{2/3}Sr_{1/3}MnO_3$	5.4489(5)	7.6910(8)	5.4525(6)	228.50(7)	0.9173	158
$(Pr_{1/3}Sm_{2/3})_{2/3}Ba_{1/3}MnO_3$	5.4949(1)	7.7740(7)	5.4937(8)	234.68(3)	0.9360	64

This indicates that the structure tends towards pseudo-cubic symmetry as one goes from Ca to Ba substituent. The cell volume decreases with decreasing A-site ionic radius.

The cells and structural parameters of all the $(Pr_{1/3}Sm_{2/3})_{2/3}A_{1/3}MnO_3$ (A = Ca, Sr and Ba) compounds were refined by the Rietveld method using the computer code FULLPROF [18]. The refinement was carried out in the space group *Pnma* (No. 62) with the following atomic positions: Pr/Sm/A: 4c(x, y, 1/4), Mn: 4b(0, 0, 1/2), O(1): 4c(x, 1/4, z) and O(2): 8d(x, y, z). The refined lattice parameters are given in table 1. The oxygen positions derived from the refinement have high errors due to the presence of strong scatterers, the Pr and Sm ions [19]. The best-fit χ^2 values for Ca-, Sr-, and Ba-substituted compounds are 2.89, 1.54 and 2.62, respectively. A typical refined pattern for one sample, namely the Sr-substituted compound, is shown in figure 2.

3.2. Electrical resistivity

The temperature dependence of the electrical resistivity, $\rho(T)$, for all the $(Pr_{1/3}Sm_{2/3})_{2/3}A_{1/3}MnO_3$ (A = Ca, Sr and Ba) compounds is shown in figure 3. The resistivity values are very high for Ca- and Ba-substituted compounds over the entire temperature range from 320 to 50 K, and these compounds show semiconducting-like behaviour ($d\rho/dT < 1$). The typical metal–insulator transition is observed only for the Sr-substituted compound.

In the Ca-substituted sample, $(Pr_{1/3}Sm_{2/3})_{2/3}Ca_{1/3}MnO_3$, a small anomaly in the $d \ln \rho/d(k_B T)^{-1}$ plot is seen around 195 K (inset of figure 3) which is a typical feature of
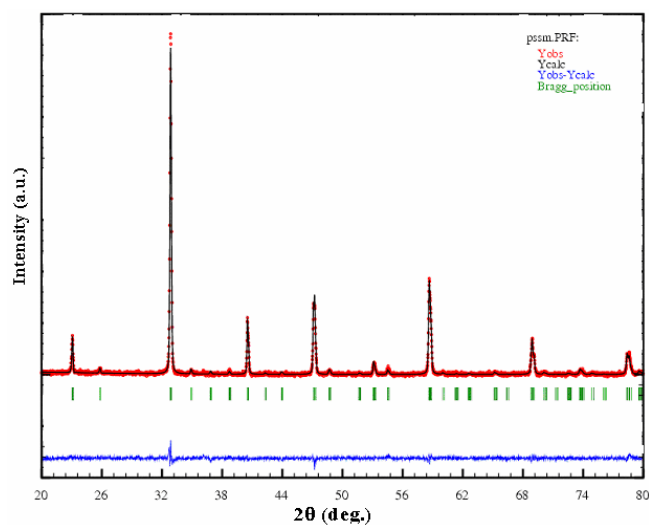
Figure 2. Rietveld refined x-ray diffraction pattern of $(Pr_{1/3}Sm_{2/3})_{2/3}Sr_{1/3}MnO_3$ using the space group *Pnma* No. 62 ($\chi^2 = 1.54$).

(This figure is in colour only in the electronic version)

charge ordering as also reported for the parent compound $Pr_{0.67}Ca_{0.33}MnO_3$ [20, 21]. It has been reported that compounds having a tolerance factor around 0.907 or less may exhibit charge order phenomena [22]. The tolerance factor for Ca-substituted sample is 0.9018, and therefore it is probably the reason for its charge ordering behaviour. As mentioned earlier, the size of the Ca^{2+} ion is smaller than those of the Ba^{2+} and Sr^{2+} ions, which in turn creates more structural distortions in the orthorhombic lattice of the Ca-substituted compound. Because of this, the Mn–O–Mn bond angle deviates more from 180° in this compound. The transfer integral (t) of the e_g electrons hopping from Mn^{3+} to Mn^{4+}, defined as $t = t_0 \cos(\theta/2)$ (where t_0 is the normal transfer integral and θ is the angle between two neighbouring spin directions [23]), reduces more drastically in the case of Ca- and Ba-substituted compounds as compared to that in the Sr-substituted compound. This leads to suppression of the DE interaction between the Mn^{3+} and Mn^{4+} and to higher resistivity values in Ca- and Ba-substituted compounds. However, the anomaly in $d \ln \rho/d(k_B T)^{-1}$ is absent in the Ba-substituted compound.

The Sr-substituted sample, $(Pr_{1/3}Sm_{2/3})_{2/3}Sr_{1/3}MnO_3$, exhibits an MI transition similar to that observed in the parent $Pr_{0.7}Sr_{0.3}MnO_3$ (PSMO) [24], but T_{MI} is shifted towards lower temperatures. The T_{MI} value for the Sr-substituted sample, estimated from the average value between minima and maxima of the $d\rho/dT$ plot, is 156 K, which is in between that of 265 K for the parent compound $Pr_{0.7}Sr_{0.3}MnO_3$ and 100 K for $Sm_{2/3}Sr_{1/3}MnO_3$ (SSMO) [25]. The drop in T_{MI} is due to the variation in the A-site ionic radius $\langle r_A \rangle$ of the compounds. The $\langle r_A \rangle$ for the Sr-substituted sample, $(Pr_{1/3}Sm_{2/3})_{2/3}Sr_{1/3}MnO_3$, is found to be 1.202 Å, which is in between the $\langle r_A \rangle$ of PSMO (1.223 Å) and SSMO (1.191 Å). The difference between the A-site ionic radius of $(Pr_{1/3}Sm_{2/3})_{2/3}Sr_{1/3}MnO_3$ and SSMO is lower (0.011 Å) as compared to that between $(Pr_{1/3}Sm_{2/3})_{2/3}Sr_{1/3}MnO_3$ and PSMO (0.021 Å). Therefore, the T_{MI} of 156 K for $(Pr_{1/3}Sm_{2/3})_{2/3}Sr_{1/3}MnO_3$ sample is closer to T_{MI} of 100 K for SSMO rather than to T_{MI} of 265 K for PSMO.

Although an MI transition is observed only in the Sr-substituted $(Pr_{1/3}Sm_{2/3})_{2/3}Sr_{1/3}MnO_3$ compound, all the $(Pr_{1/3}Sm_{2/3})_{2/3}A_{1/3}MnO_3$ (A = Ca, Sr and Ba) compounds show a
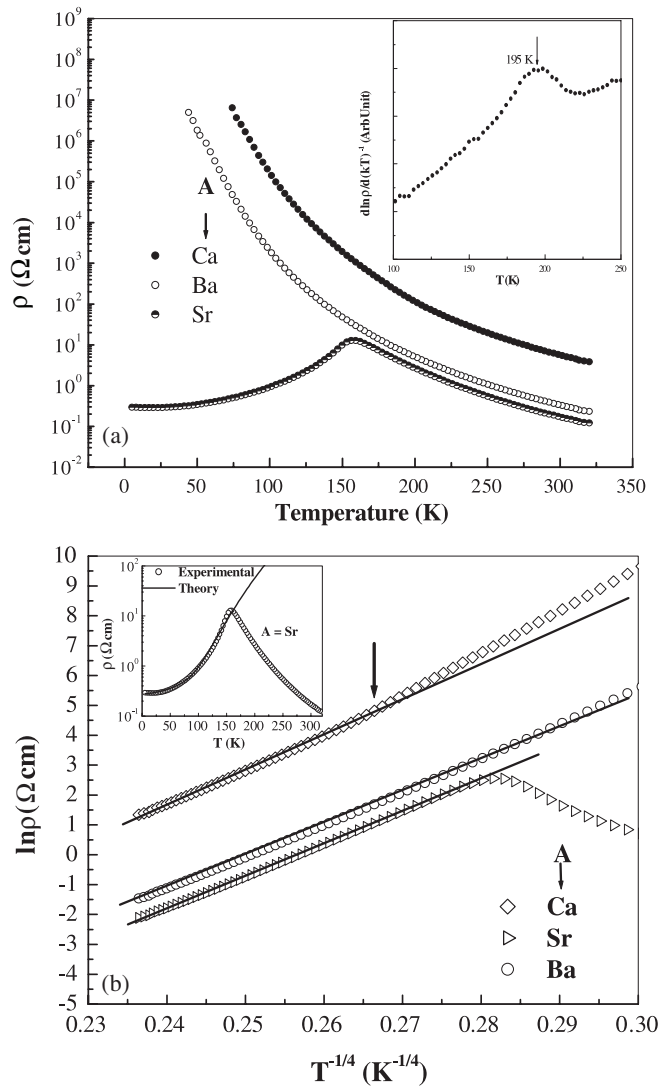
Figure 3. (a) Variation of resistivity with temperature for $(Pr_{1/3}Sm_{2/3})_{2/3}A_{1/3}MnO_3$ (A = Ca, Sr and Ba). The $d\ln\rho/d(k_BT)^{-1}$ versus T plot for Ca-substituted $(Pr_{1/3}Sm_{2/3})_{2/3}Ca_{1/3}MnO_3$ (inset) shows the anomaly at the charge order temperature (marked by an arrow). (b) Theoretical fit of the transport data using the Mott VRH model for $(Pr_{1/3}Sm_{2/3})_{2/3}A_{1/3}MnO_3$ (A = Ca, Sr and Ba). The charge ordering point in the Ca-substituted system is indicated by an arrow. The inset shows the theoretical fit of the transport data for the Sr-substituted system in the metallic regime.

paramagnetic (PM) to ferromagnetic (FM) transition (see the magnetization section). In the Sr-substituted $(Pr_{1/3}Sm_{2/3})_{2/3}Sr_{1/3}MnO_3$ compound, T_{MI} and T_C are very close to each other, which is evidence of long range ferromagnetism. Thus for the Ba- and Ca-substituted compounds (where an MI transition is not observed), long range ferromagnetism, due to double exchange, disappears and consequently hinders metallicity, leading to a monotonic increase in resistivity [26].

The transport data in the semiconducting regime of $(Pr_{1/3}Sm_{2/3})_{2/3}A_{1/3}MnO_3$ (A = Ca, Sr and Ba) compounds has been analysed by the Mott variable range hopping (Mott-VRH)

Table 2. Parameters obtained from experimental and theoretical analysis.

Systems	$(Pr_{1/3}Sm_{2/3})_{2/3}Ca_{1/3}MnO_3$	$(Pr_{1/3}Sm_{2/3})_{2/3}Sr_{1/3}MnO_3$	$(Pr_{1/3}Sm_{2/3})_{2/3}Ba_{1/3}MnO_3$
T_{MI}/T_{CO} (K)	$T_{CO} = 195$	$T_{MI} = 156$	—
$\rho_{300\ K}$ (Ω cm)	5.42	0.17	0.32
ρ_0 (Ω cm)	—	0.28	—
ρ_2 (Ω cm K^{-2})	—	3×10^{-5}	—
$\rho_{7.2}$ (Ω cm K$^{-7.2}$)	—	1.5×10^{-15}	—
ρ_{0m} (Ω cm)	1.60	0.05	0.11
T_{0m} ($\times 10^8$ K)	1.72	1.62	1.57

model [27], according to which

$$\rho = \rho_{0m} \exp(T_{0m}/T)^{1/4}. \tag{1}$$

Here ρ_{0m} is the Mott residual resistivity and T_{0m} is the Mott characteristic temperature. Equation (1) is found to fit the data well, as is shown in figure 3(b). The values of ρ_{0m} and T_{0m} are listed in table 2. A small deviation in theoretical fit is observed in the Ca-substituted system at the charge ordering temperature ($T_{CO} = 195$ K), as indicated by arrow in figure 3(b).

The metallic region in the Sr-substituted $(Pr_{1/3}Sm_{2/3})_{2/3}Sr_{1/3}MnO_3$ system has been fitted to a Zener double-exchange polynomial

$$\rho = \rho_0 + \rho_2 T^2 + \rho_n T^n, \tag{2}$$

where ρ_0 is the temperature independent residual resistivity due to scattering by impurities, defects, grain boundaries and domain walls. The second term with coefficient ρ_2 is ascribed to the electron–electron and electron–phonon scattering mechanism [28], and the third term with coefficient ρ_n corresponds to the electron–magnon scattering [27]. The value of n is found to be 7.2 in the Sr-substituted system. The fitted plot is shown in the inset of figure 3(b). The typical fitted parameters are summarized in table 2.

3.3. Magnetoresistance

Figure 4(a) shows the electrical resistivity behaviour of the Sr-substituted $(Pr_{1/3}Sm_{2/3})_{2/3}Sr_{1/3}$ MnO_3 sample in different applied magnetic fields. In the presence of an external field, the resistivity decreases significantly, and T_{MI} shifts to a higher value, from 156 K in zero field to 192 K in 8 T field. This suggests that the external magnetic field facilitates the hopping of e_g electrons between neighbouring Mn ions, which agrees with the DE model [29]. The magnetoresistance (MR) is defined as

$$\%MR = 100 \times [\rho(H, T) - \rho(0, T)]/[\rho(0, T)], \tag{3}$$

where $\rho(H, T)$ and $\rho(0, T)$ are the resistivities at a temperature T, in applied magnetic field H and in zero applied magnetic field, respectively. The temperature dependence of the MR for the Sr-substituted compound is shown in figure 4(b). The MR is quite high (>95% at 8 T) at the MI transition temperature. The manganese ions are ferromagnetically ordered below T_C; therefore, within a single magnetic domain, the e_g electron transfer between Mn^{3+} and Mn^{4+} ions is easy. The pairs of Mn^{3+} and Mn^{4+} spins, which may not be parallel in the vicinity of domain wall boundaries, will act as a hindrance for electron transport. The magnetic domains tend to align along the field direction in the presence of sufficiently strong magnetic field. As a result, hopping of electrons become easy across the domain wall boundaries and the resistivity decreases, which in turn leads to significant MR at low temperatures. Unlike in La$_{2/3}$Sr$_{1/3}$MnO$_3$, the MR in Sr-substituted compound does not drop to a low value at low
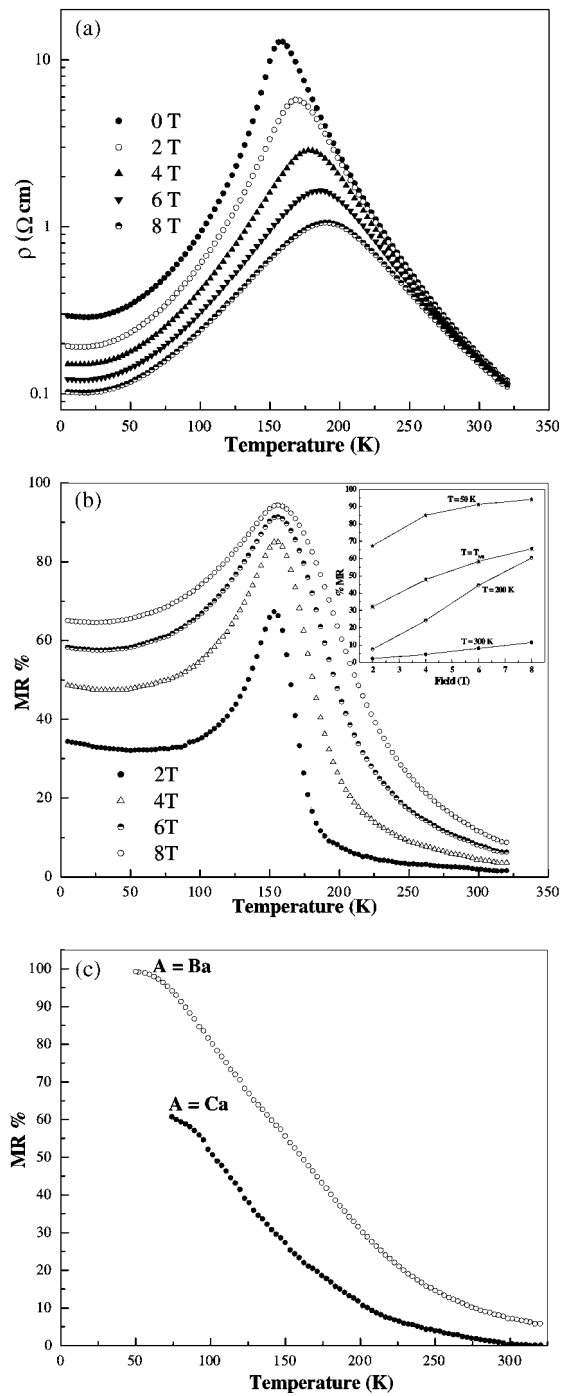
Figure 4. (a) Variation of resistivity with temperature at different fields for the Sr-substituted $(Pr_{1/3}Sm_{2/3})_{2/3}Sr_{1/3}MnO_3$, sample. (b) Variation of negative MR% with temperature for the Sr-substituted $(Pr_{1/3}Sm_{2/3})_{2/3}Sr_{1/3}MnO_3$ sample. The field dependence of MR at different temperatures is shown in the inset. (c) Variation of negative MR% with temperature for $(Pr_{1/3}Sm_{2/3})_{2/3}A_{1/3}MnO_3$ (A = Ba and Ca) samples.

temperatures but rather remains high and weakly temperature dependent below 100 K due to the intergrain tunnelling at low temperatures [15].

The temperature dependence of the MR for Ba- and Ca-substituted $(Pr_{1/3}Sm_{2/3})_{2/3}$ $A_{1/3}MnO_3$ compounds is shown in figure 4(c). It is remarkable to note that for the Ba-substituted sample, the MR is ∼99% at low temperatures in 8 T magnetic fields while it is around 60% for the Ca-substituted sample, though the temperature dependence of the MR exhibits similar nature in the two. The continuous rise in MR with decreasing temperature and its large value in Ba- and Ca-substituted samples appear to be due to electronic phase separation, where presumably the ferromagnetic (FM) clusters start growing at the expense of antiferromagnetic clusters with decreasing temperature in a high field of 8 T. Similar MR behaviour has been observed in $(La_{0.6}Ho_{0.4})_{0.7}Sr_{0.3}MnO_3$ [30].
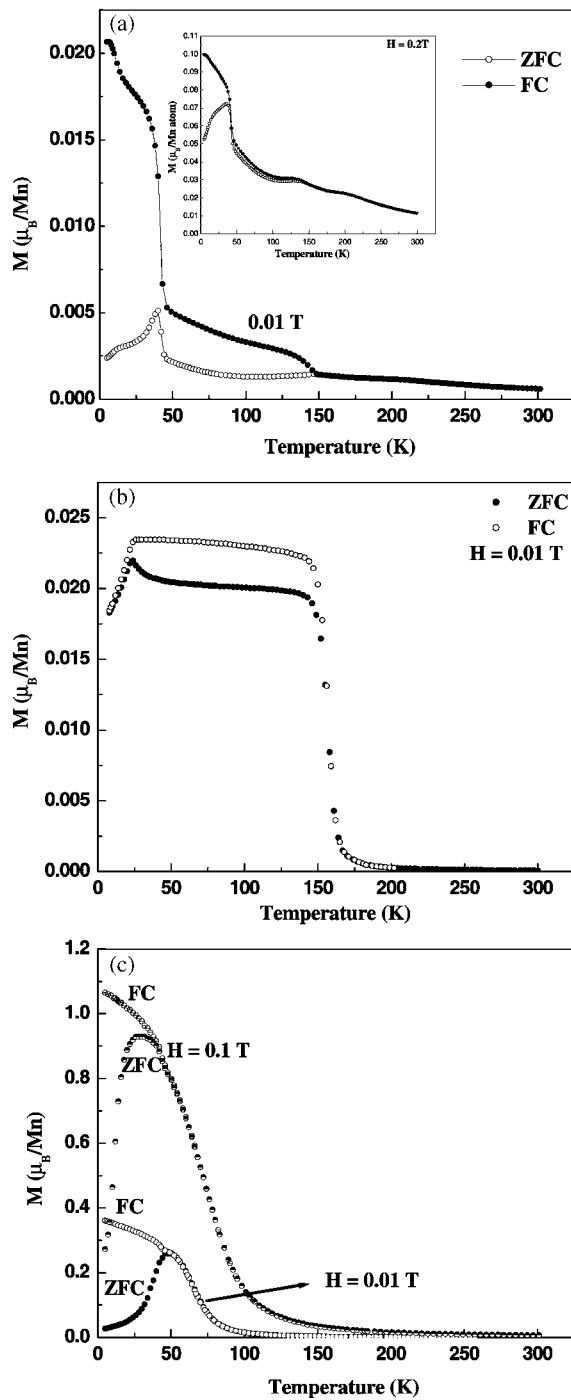
3.4. Magnetization

Plots of magnetization (M) as a function of temperature (T) for $(Pr_{1/3}Sm_{2/3})_{2/3}A_{1/3}MnO_3$ (A = Ca, Sr and Ba) compounds are shown in figures 5(a)–(c). In the Ca-substituted sample, at low fields (0.01 T), the magnetization (M) shows irreversibility between the zero-field cooled (ZFC) and the field cooled (FC) state below 150 K. This irreversibility becomes very strong below around 40 K. At higher field (above 0.2 T), as shown in the inset of figure 5(a), the irreversibility is observed only below 40 K. The magnetic transition temperatures have been determined from the minima in the dM/dT plots. In $Pr_{0.65}Ca_{0.35}MnO_3$, a charge ordering (CO) transition at 230 K followed by an AF transition around 165 K has been reported [31]. In the Ca-substituted sample, $(Pr_{1/3}Sm_{2/3})_{2/3}Ca_{1/3}MnO_3$, we observe a weak signature of an AF transition below 150 K, where also the setting in of irreversibility between ZFC and FC magnetization is seen. The appearance of irreversibility in M could be attributed to magnetic frustration generated due to competing FM and AFM moments as found in the neutron diffraction studies on $Pr_{0.7}Ca_{0.3}MnO_3$ [32].
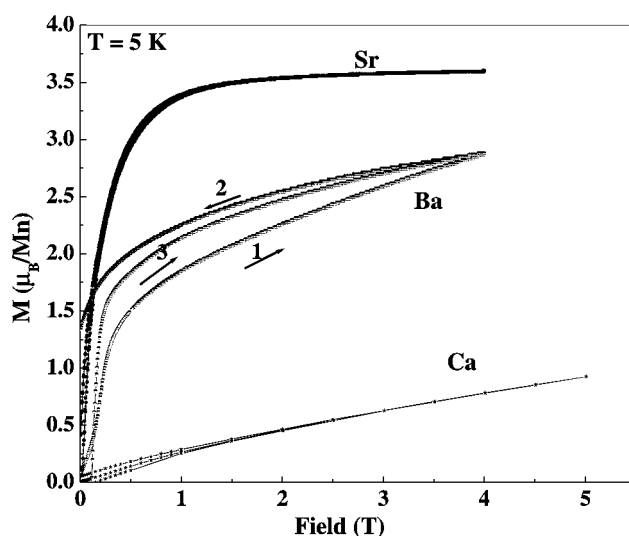
For the Ba-substituted $(Pr_{1/3}Sm_{2/3})_{2/3}Ba_{1/3}MnO_3$ sample, the irreversibility between ZFC and FC magnetization is seen below 50 K both in 0.01 and 0.1 T field (figure 5(c)). This behaviour is similar to that found in cluster glasses. In the case of the Sr-substituted sample, a ferromagnetic transition is observed at $T_C = 158$ K (figure 5(b)), which is the same as the MI transition temperature in zero field. Below T_C, irreversibility between ZFC and FC magnetization is observed, which could be due to domain wall pinning. Further, below around 25 K, $M(T)$ drops, presumably due to competing superexchange and double exchange interactions resulting in the formation of localized spin clusters.

Figure 6 shows the isothermal magnetization at 5 K for $(Pr_{1/3}Sm_{2/3})_{2/3}A_{1/3}MnO_3$ (A = Ca, Sr and Ba) compounds. The magnetization of the Sr-substituted compound shows near saturation, and its value is 3.62 μ_B/Mn, which is close to the theoretical value (3.7 μ_B/Mn). The magnetization of Ba- and Ca-substituted samples does not saturate even in a field of 4 T. The Ba-substituted sample shows a large remanence in $M(H = 0)$ indicating the presence of a strong FM phase in it. Non-saturating near-linear behaviour is observed in the Ca-substituted system at 5 K even up to 5 T magnetic field, which is expected in an AF or spin-glass-like state. Non-saturating $M–H$ behaviour for Ca- and Ba-substituted samples may also result from the presence of well-separated charge delocalized ferromagnetic clusters in the antiferromagnetic insulating matrix [33]. These clusters start growing within the matrix with increasing magnetic field.

The field dependence of magnetization as shown in figure 6 supports the MR behaviour, i.e. the Sr-substituted sample is ferromagnetic, the Ba-substituted sample has a spin-glass (or cluster-glass) type of disorder giving rise to a non-saturating behaviour even at 8 T.

Figure 5. (a) Temperature dependence of magnetization in a field of 0.01 T in ZFC and FC runs for the Ca-substituted $(Pr_{1/3}Sm_{2/3})_{2/3}Ca_{1/3}MnO_3$, sample. The inset shows the $M(T)$ plot in a field of 0.2 T for the same sample. (b) FC and ZFC magnetization plots for the Sr-substituted $(Pr_{1/3}Sm_{2/3})_{2/3}Sr_{1/3}MnO_3$ sample in a field of 0.01 T. (c) Variation of magnetization with temperature for the Ba-substituted $(Pr_{1/3}Sm_{2/3})_{2/3}Ba_{1/3}MnO_3$ sample in fields of 0.01 and 0.1 T.

Figure 6. The isothermal variation of magnetization with field for the series $(Pr_{1/3}Sm_{2/3})_{2/3}A_{1/3}MnO_3$ (A = Ca, Sr and Ba) at 5 K.

(Presumably in this compound electronic phase separation is quite significant.) In the Ca-substituted compound, the charge ordered state is much more robust, having a nearly AF state. However, the large MR ($\sim$60%) at low temperature suggests that there is electronic phase separation in this compound too.

4. Conclusions

We have investigated the effect of alkaline earth ion substitution on the structural and magneto-transport properties of $(Pr_{1/3}Sm_{2/3})_{2/3}A_{1/3}MnO_3$ (A = Ca, Sr and Ba) compounds. Synthesized samples crystallize in the orthorhombic structure (space group *Pnma* No. 62). The Ba- and Ca-substituted $(Pr_{1/3}Sm_{2/3})_{2/3}A_{1/3}MnO_3$, (A = Ca and Ba) samples show an insulating behaviour. However, a small anomaly due to charge ordering is observed around 195 K for the Ca-substituted sample only. Unlike Ba- and Ca-substituted samples, the Sr-substituted sample shows a metal-to-insulator transition. Spin-glass/cluster-like behaviour is observed in Ca- and Ba-substituted samples, which is also supported by the non-saturating behaviour in M–H plots. The non-saturating MR value at low temperatures is observed in the case of Ca- and Ba-substituted samples. In addition, the Ba-substituted sample exhibits a very high MR ($\sim$99%) in 8 T magnetic field. The magnetic behaviour is attributed due to electronic phase separation.

Acknowledgment

References

[1] Heremans J 1993 *J. Phys. D: Appl. Phys.* **26** 1149
[2] Jin S, McCormack M, Tiefel T H and Ramesh R 1994 *J. Appl. Phys.* **76** 6929

[3] Srivastava C M, Banerjee S, Gundu Rao T K, Nigam A K and Bahadur D 2003 *J. Phys.: Condens. Matter* **15** 2375

[4] Verma D, Nigam A K, Gundu Rao T K and Bahadur D 2004 *J. Magn. Magn. Mater.* **271** 172

[5] Das D, Raj R, Srivastava C M, Bahadur D, Nigam A K and Malik S K 2004 *J. Phys.: Condens. Matter* submitted

[6] Millis A J, Littlewood P B and Shraiman B I 1995 *Phys. Rev. Lett.* **74** 5144

[7] Mahesh R, Mahendiran R, Raychaudhuri A K and Rao C N R 1995 *J. Solid State Chem.* **114** 297

[8] Damay F, Martin C, Martin A and Raveau B 1997 *J. Appl. Phys.* **81** 1372

[9] Rodriguez-Martinez L M and Attfield J P 1996 *Phys. Rev.* B **54** 15622

[10] Damay F, Martin C, Maignan A and Raveau B 1997 *J. Appl. Phys.* **82** 6181

[11] Troyanchuk I O, Trukhanov S V, Szymezak H and Baerner K 2000 *J. Phys.: Condens. Matter* **12** L155

[12] Millis A J 1997 *J. Appl. Phys.* **81** 5502

[13] Sudheendra L and Rao C N R 2003 *J. Phys.: Condens. Matter* **15** 3029

[14] Das D, Chowdhury P, Das R N, Srivastava C M, Nigam A K and Bahadur D 2002 *J. Magn. Magn. Mater.* **238** 178

[15] Das D, Saha A, Russek S E, Raj R and Bahadur D 2003 *J. Appl. Phys.* **93** 8301

[16] Attfield J P 2002 *Crys. Eng.* **5** 427

[17] Shannon R D 1976 *Acta Crystallogr.* A **32** 751

[18] Rodríguez-Carvajal J 2001 *FULLPROF* version 2001, Laboratoire Léon Brillouin (CEA-CNRS)CEA/Saclay, 91191 Gif sur Yvette Cedex, France

[19] Collado J A, Frontera C, Garcia Munoz J L, Ritter C, Brunelli M and Aranda M A G 2003 *Chem. Mater.* **15** 167

[20] Jardon C, Rivadulla F, Hueso L E, Fondado A, Lopez-Quintela M A, Rivas J, Zysler R, Causa M T and Sanchez R D 1999 *J. Magn. Magn. Mater.* **196/197** 475

[21] Rivadulla F, Lopez-Quintela M A, Hueso L E, Jardon C, Fondado A, Rivas J, Causa M T and Sanchez R D 1999 *Solid State Ion.* **110** 179

[22] Tokura Y 2000 *Colossal Magnetoresistive Oxides* (Amsterdam: Gordon and Breach)
Rao C N R and Raveau B 1998 *Colossal Magnetoresistance, Charge Ordering and Related Properties of Manganese Oxides* (Singapore: World Scientific)

[23] Coey J M D and Viret M 1999 *Adv. Phys.* **48** 167

[24] Abou-Ras D, Boujelben W, Cheikh-Rouhou A, Pierre J, Renard J-P, Reversat L and Shimizu K 2001 *J. Magn. Magn. Mater.* **233** 147

[25] Caignaert V, Maignan A and Raveau B 1995 *Solid State Commun.* **95** 357

[26] Maignan A, Martin C, Van Tendeloo G, Hervieu M and Raveau B 1999 *Phys. Rev.* B **60** 15214

[27] Rana D S, Thaker C M, Mavani K R, Kubekar D G, Kundaliya D C and Malik S K 2004 *J. Appl. Phys.* **95** 4934

[28] Ziese M 2000 *Phys. Rev.* B **62** 1044

[29] Zener C 1951 *Phys. Rev.* **82** 403
de Gennes P G 1960 *Phys. Rev.* **118** 141

[30] Raychaudhuri P, Nath T K, Sinha P, Mitra C, Nigam A K, Dhar S K and Pinto R 1997 *J. Phys.: Condens. Matter* **9** 10919

[31] Kajimoto R, Kakeshita T, Oohara Y, Yoshizawa H, Tomioka Y and Tokura Y 1998 *Phys. Rev.* B **58** R11837

[32] Cox D E, Radaelli P G, Marezio M and Cheong S-W 1998 *Phys. Rev.* B **57** 3305

[33] Li G, Xianyu Z, Kim C O, Kim H J and Lee Y W 2002 *J. Magn. Magn. Mater.* **239** 51